Vlastimil Vondra*, Pavel Jurak, Ivo Viscor, Josef Halamek, Pavel Leinveber, Magdalena Matejkova and Ladislav Soukup

# A multichannel bioimpedance monitor for full-body blood flow monitoring

**Abstract:** The design, properties, and possible diagnostic contribution of a multichannel bioimpedance monitor (MBM) with three independent current sources are presented in this paper. The simultaneous measurement of bioimpedance at 18 locations (the main part of the body, legs, arms, and neck) provides completely new information, on the basis of which more precise haemodynamic parameters can be obtained. The application of the MBM during various haemodynamic stages, such as resting in a supine position, tilting, exercise stress, and various respiration manoeuvres, is demonstrated. Statistical analysis on a group of 34 healthy volunteers is presented for demonstration of blood flow monitoring by using the proposed method.

**Keywords:** bioimpedance; blood flow; cardiac output; non-invasive measurement; pulse wave velocity; simultaneous multichannel measurement.

DOI 10.1515/bmt-2014-0108
Received September 12, 2014; accepted April 17, 2015; online first May 20, 2015

## Introduction

Disease of the heart and blood vessels is one of the most frequent causes of sudden cardiac death and has a serious impact on the state of health today. Early diagnosis of the haemodynamic system could play an important role in follow-up patient treatment. The important parameters describing haemodynamics are stroke volume (SV), cardiac output (CO), and blood circulation or vessel elasticity. SV represents the volume of blood pumped from the left and right ventricles of the heart with each beat. CO is the volume of blood pumped during a time interval of 1 min. The non-invasive measurement of these fundamental haemodynamic parameters is complicated and inaccurate. One of the methods used for measuring SV and CO is thoracic impedance cardiography (ICG). ICG estimates cardiac function from a single impedance waveform measured at the thorax surface that reflects an integrated combination of complex thoracic sources. The first practical method for the determination of cardiac function in a clinical setting was introduced by Kubicek et al. in the 1960s [15]. The evaluation of SV and CO from ICG has evolved from the former Kubicek equation to the Sramek equation and finally to the Bernstein equation [1, 2, 17], and would seem to be developing further to use not only changes in electric resistance but also electric reactance [11]. The position of the electrodes [6] and the combination of two bioimpedance channels [14, 21] are also being researched to improve the quality of the results. A new and more accurate technique of estimating CO, called transbrachial electrical bioimpedance velocimetry, was introduced by Henry et al. [9]. Bioimpedance is also used for many other purposes, such as impedance spectroscopy and three-dimensional electrical impedance tomography [3, 16, 20, 24]. These methods do not map the dynamics of blood flow, but they can be used as diagnostic tools for specific diseases. Measurement of two impedance channels is used for pulse wave velocity (PWV) calculation between the chest and calf [13].

Bioimpedance methods initially suffered from bad signal quality. Also, these methods do not have a good reputation because of poor accuracy in the evaluation of the absolute values of parameters. This is caused mainly by the excessive influence of bioimpedance signals from the chest – breathing, muscle contraction, and the combination of several pieces of information together (aorta, pulmonary aorta, abdominal aorta, lung filling). The

***Corresponding author: Vlastimil Vondra,** Institute of Scientific Instruments of the ASCR, v.v.i., Academy of Sciences of the Czech Republic, Královopolská 147, 612 64 Brno, Czech Republic, Phone: +420 541514310, Fax: +420 541514402, E-mail: vond@isibrno.cz; and International Clinical Research Center, St. Anne's University Hospital Brno, Pekařská 53, 656 91 Brno, Czech Republic
**Pavel Jurak and Josef Halamek:** Institute of Scientific Instruments of the ASCR, v.v.i., Královopolská 147, 612 64 Brno, Czech Republic; and International Clinical Research Center, St. Anne's University Hospital Brno, Pekařská 53, 656 91 Brno, Czech Republic
**Ivo Viscor:** Institute of Scientific Instruments of the ASCR, v.v.i., Královopolská 147, 612 64 Brno, Czech Republic
**Pavel Leinveber, Magdalena Matejkova and Ladislav Soukup:** International Clinical Research Center, St. Anne's University Hospital Brno, Pekařská 53, 656 91 Brno, Czech Republic

results are also highly dependent on the patient's own physical parameters and the condition of his or her arteries [10]. Poor bioimpedance signals from some monitors may also make any reasonable results impossible. All of the above-mentioned phenomena influence the evaluation of the absolute calibrated values of SV and CO. However, relative changes in haemodynamic parameters can be monitored more sensitively without additional artificial coefficients. This leads to a lack of belief in this method, and several methods, both non-invasive and invasive, are used for CO calculation (echocardiography, thermodilution).

Great progress in digital signal processing hardware has enabled improvements in the quality of impedance and, therefore, improvements in the accuracy and reliability of blood flow measurement. Several commercial companies produce clinical CO monitors [8, 18], which means that the bioimpedance-based method has become more acceptable among physicians and professionals. Many studies have been published comparing bioimpedance-based methods with other methods for CO measurement [7, 12, 19, 23]. Although a "gold standard" exists (the thermodilution method), there is no universal method that is best in all cases [7].

The basic idea of the multichannel bioimpedance monitor (MBM; ISIBRNO MPM 14.1, Institute of Scientific Instruments, Brno, Czech Republic) is to measure bioimpedance in the body, extremities, and neck simultaneously and independently. A similar device with multichannel capability in only one extremity is presented in Ref. [4]. The used principle cannot be extended to full-body measurements without crosstalk among channels. The MBM uses three independent current sources operating at different frequencies – three current generators with adjustable frequency and amplitude. The MBM can cover the desired number of scanning channels that enable the detection exclusively of those signals for which the frequency is adjusted. The scanning electrodes can be placed according to the desired localisation. Full-body coverage, which takes in as many as 18 localisations, provides additional information for the analysis of dynamic changes of SV and blood circulation. Moreover, the impedance signal from the extremities and neck measured during steady states, excitations, and manoeuvres significantly expands the diagnostic possibilities. A new method of vessel resistance and compliance may be designed on this basis.

We are concentrating here on describing the principle of the system and a technical solution that can provide high-quality impedance data for further evaluation. A passing mention of the processing of the impedance signal is given in the examples covering a group of 34 subjects.

# Methods

The MBM monitor consists of separate modules including three individually adjustable current generators and 18 impedance-scanned channels. The combination and setting of these modules can be configured to any type of multichannel impedance measurement.

### Impedance measurement method and patient connection

We used a four-electrode method for the measurement of the bioimpedance signal from the desired part of the body. This method is identical with the method used for CO measurement on the chest. The alternating sine wave current source $I_i$ ($t$) is connected to the outer electrodes (current electrodes), and the voltage-sensing channel CH j (voltage electrodes) is connected to the inner electrodes. The four-electrode system is used to eliminate the influence of the intrinsic impedance of the electrodes and skin-electrode impedance. The impedance $Z_j(t)$ of the selected part of the body (channel j) between electrodes CH j+ and CH j- can be calculated with the help of the Ohm's law equation:

$$Z_j(t) = U_j(t) / I_i(t),$$

where $U_j(t)$ is the voltage measured between electrodes CH j+ and CH j-. In general, this impedance is a complex value and can be written in component or polar forms – see the equation below:

$$Z_j(t) = R_j(t) + iX_j(t) = |Z_i(t)| e^{i\phi_j(t)},$$

where $R_j(t)$ and $X_j(t)$ are the real and imaginary part of impedance, $|Z_j(t)|$ and $\phi_j$ ($t$) are the magnitude and the phase of impedance of channel j.

This principle is applicable to any part of the body. For the purpose of investigating blood flow in the body, it is necessary to choose a part of the body that includes major arteries in which heart activity causes meaningful changes in impedance that are significant for flow evaluation.

Spatial definition of a body part is defined by the placement of voltage electrodes on the proper part of the body. The voltage signal then corresponds to the section between a particular pair of voltage electrodes CH j. The proposed placement of electrodes is depicted in Figure 1. On the neck, we chose part of the left and right carotid (CH 1 and CH 2), on the chest the left and right part (CH 3 and CH 4), the left and right upper part of the chest (CH 11 and CH 12), and the left and right part of the chest at the level of the heart (CH 17 and CH 18). The abdomen was monitored on the left and right parts together with the abdominal artery (CH 9 and CH 10), and electrodes were placed on the back at the level of the T9 and L9 vertebra. On the upper extremity, the electrodes were on the inner side of the arm (CH 13 and CH 14) and the forearm (CH 15 and CH 16). The lower extremities were measured at the left and right thighs (CH 5 and CH 6) and calves (CH 7 and CH 8).

Because of the complexity of the constitution of the human body, it is impossible to use just one constant current source. We use three current sources that can cover almost all of the mentioned parts of the body. Constant current source $I_1$ was intended to measure the impedance of the left side of the body. One of its current electrodes is attached to the head above the first scanning point and behind the left ear; the other current electrode is attached below the last

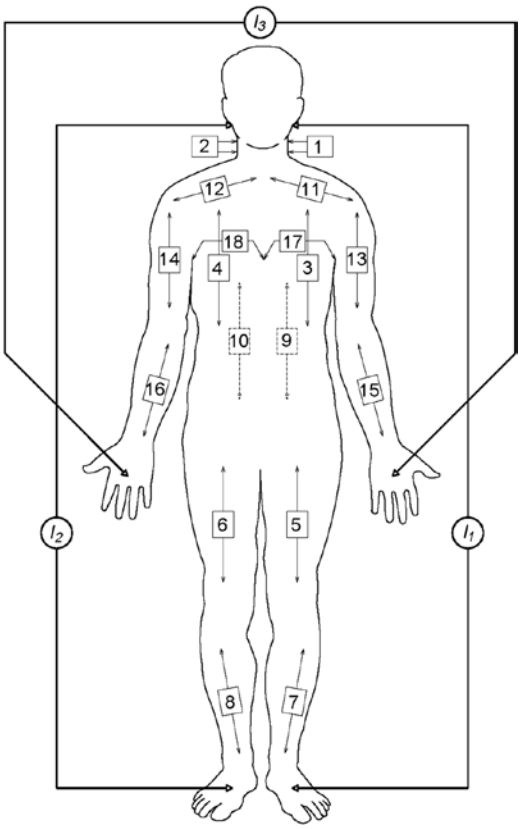


**Figure 1:** Placement and connection of the voltage and current electrodes for the selection of human body part.

scanning point on the instep of the left foot. The $I_1$ current flowed from the left ear through the chest into the left leg and down to the instep. A similar connection is used for constant current source $I_2$, but it is connected to the right part of the body. Current source $I_3$ is intended to measure the impedance of the upper limbs and the upper and middle part of the chest. One of the current electrodes is attached before the first scanning point on the back of the left hand; the other current electrode is attached after the last scanning point on the back of the right hand. The $I_3$ current therefore flows from the left palm through the left arm and the chest into the right arm and down to the palm. The human body is conductive, and all three current sources may influence each other. To prevent this, we have proposed using a different frequency for each current source and the use of galvanic insulated current sources. The frequencies $f_1$, $f_2$, and $f_3$ of $I_1$, $I_2$, and $I_3$ must be different; however, these differences should be as small as possible in order to retain the same properties of impedance measurement in the full body. All the scanning channels CH j are tuned to the proper frequency. Channels CH 1, CH 3, CH 5, CH 7, and CH 9 are tuned to frequency $f_1$; channels CH 2, CH 4, CH 6, CH 8, and CH 10 are tuned to frequency $f_2$; and channels CH 12, CH 13, CH 14, CH 15, CH 16, CH 17, and CH 18 are tuned to frequency $f_3$. The frequency bandwidth B j of each channel CH j must be sufficiently narrow so as not to acquire information from other frequencies. The final frequency bandwidth chosen is 250 Hz for each channel, and the difference between current source frequencies is 1 kHz to meet these demands. The situation is outlined in Figure 2. This solution, consisting of the spatial placement of scanning channel electrodes with the proper design of current circuits and setting of frequencies

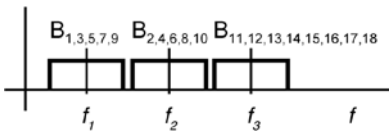


**Figure 2:** Frequency of constant current sources and frequency bandwidth of scanning channels.

of current sources and frequency tuning of scanning channels, ensures that the information in each channel is separated from all others. All the channels are measured simultaneously, so impedance information is available at all times and in all channels.

## Implemented impedance estimation

The heartbeat invokes modulation of the basic impedance, and the variation, therefore, is extremely weak relative to basic impedance and to the variation given by breathing and body position. Demodulation with a high dynamic range is required to obtain information about impedance changes induced by blood flow. The principal concept of the impedance monitor module is constructed with a digital synthesiser, and direct coherent digital demodulation is depicted in Figure 3. The device consisted of three sine wave current generators, comprising three alternating-current sources $I_1$, $I_2$, and $I_3$ with frequencies $f_1$, $f_2$, and $f_3$, and 18 input channels each tuned to the desired frequency $f_1$, $f_2$, or $f_3$. The sine wave is computed in the numerically controlled oscillator (NCO) and transferred to the analogue domain by a digital-to-analogue converter (DAC). The signal from the electrodes is digitised by an analogue-to-digital converter (ADC) and multiplied by quadrature sine waves from the NCO. The resulting complex envelope is digitally filtered by a low-pass filter. The in-phase component represents the resistance $R$, and the quadrature component represents the reactance $X$ of the measured impedance. By this procedure, the signal of each channel is frequency shifted to the zero frequency. The principle of the signal measurement and processing is described in Ref. [22]. For further PWV calculation, only the magnitude of an impedance is used.

In the practical design of the monitor module, there is a separate NCO for the current generator and for each detection channel. All those oscillators use the same clock and are synchronised to achieve virtually a single NCO. The monitor is based on signal processing in high-integrated chips (see Figure 4). The direct digital synthesiser (DDS) chip integrates the NCO and DAC. The digital receiver

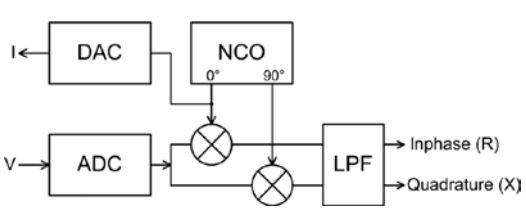


**Figure 3:** Measurement of impedance using direct digital synthesis and digital quadrature detection.
DAC, digital-to-analog converter; ADC, analog-to-digital converter; NCO, numerically controlled oscillator; LPF, low-pass filter; R, resistance; X, reactance; I, current; V, voltage.

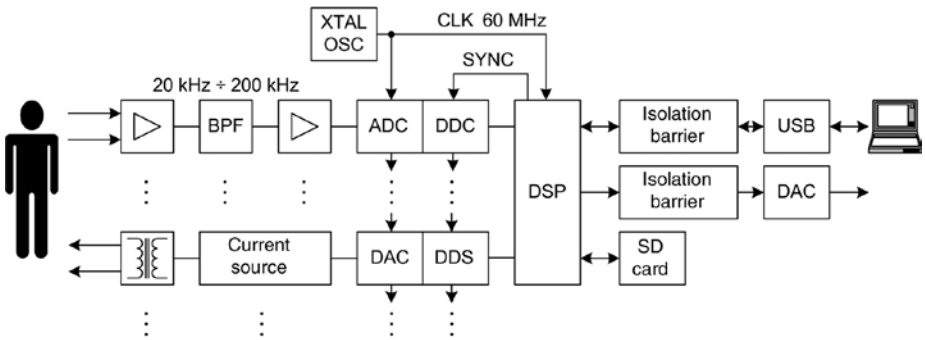


**Figure 4:** Block diagram of multichannel bioimpedance measurement system.
BPF, band pass filter; ADC, analog to digital converter; DDC, digital down converter; DSP, digital signal processor; DAC, digital to analog converter; DDS, direct digital synthesizer; SD, secure digital; XTAL OSC, crystal oscillator.

chip integrates the ADC and digital down-conversion (DDC) – i.e., NCO, digital multiplication, and filtration.

The unit is controlled by a fixed-point digital signal processor (DSP). The digitally generated sine wave drives the current source. The current source is represented by one operational amplifier that is connected in circuit as a voltage-controlled current source [5]. One feedback resistor serves as a current sensor, and it is connected in series with an output transformer. The output transformer makes the current output isolated and balanced. An instrumentation amplifier amplifies the voltage drop on the measured impedance, and the signal is frequency-limited by a filter. The filter suppresses the DC offset and possible out-of-band interference, both of which can degrade the effective dynamic range of the monitor. The subsequent amplifier differentially drives the ADC that is sampling at 60 MHz. The highly integrated digital receiver chip AD6652 is composed of two 12-bit ADC channels and four DDC channels, two of which are unused. The demodulated zero-frequency signal is filtered and decimated by 6000 in the DDC. The resulting 16-bit complex envelope with a bandwidth of 10 kHz is read by DSP. The DSP writes impedance data in real time to a PC via a USB. Optional storage to an SD/SDHC card and analogue output of the impedance signal are also possible.

In order to assure perfect phase coherence of the monitor, the DDS, DDC, and DSP utilise the same clock in all channels. The common clock and the synchronisation signal also guarantee the precise start and end of the measurement.

The monitor unit is powered from an NiMH accumulator or from an external power supply through a DC/DC converter with safety approval in order to comply with patient safety standards. The measurement current is set to 1 mA. Safety serial resistors for voltage and current electrodes are implemented. The digital output to PC and analogue output are insulated from the unit by a digital isolator with safety approval.

The MBM parameters were as follows: current source frequency 2–500 kHz, number of channels up to 20, wideband ($\Delta f$>200 Hz) dynamic range of 121 dBc/√Hz, phase resolution better than 0.001°, output data format 16-bit complex envelope at 10 kHz sampling finally resampled to 500 Hz, and battery operation time up to 3 h. The two-tone (49 kHz, 50 kHz) intermodulation distortion appearing in worst-case separation of channels on different frequencies is better than 56 dB. The device was set for measurement as follows: 18 scanned channels and three sine wave current generators with frequencies $f_1$=49 kHz, $f_2$=50 kHz, and $f_3$=51 kHz, with current RMS=1 mA. Simultaneously with 18 MBM channels, we measured 12-lead ECG (ISI BRNO ECG12, Institute of Scientific Instruments, Brno, Czech Republic), continuous blood pressure (BP) (Finapres-2300, Ohmeda Medical, Englewood, CO, USA), and phonocardiography (ISI BRNO PCG 1.0, Institute of Scientific Instruments, Brno, Czech Republic), all with a sampling frequency of 500 Hz. The impedance signal time series of MBM were obtained as complex numbers.

## Processing the impedance signal

The different shapes of the impedance signal at different locations reflect both the dynamic changes in vascular volume during one heartbeat and long-term vascular volume change during excitations.

The PWV can be easily defined in various parts of the human body:

$$\text{PWV i-j}=\textit{distance}\ \text{j-i}/(t\_\text{-d}Z/\text{d}t\text{maxj-}t\_\text{-d}Z/\text{d}t\text{maxi}),$$

where PWV i-j means the PWV between channels i and j, $t\_$-d$Z$/d$t$maxj is the time position of the maximum of the negative derivative of magnitude of impedance of channel j (similarly for channel i), and the *distance* j-i is the distance of centres allocated by the voltage electrodes of channels i and j. Channels i and j should have common arteries or, in other words, they should lie on the same pathway of blood flow; otherwise, the PWV is not meaningful. As it is usually done, the PWV is calculated between the chest and the left or right leg. This corresponds to PWV 3-7 or PWV 4-8. For simplicity, we can set only one signal from the chest by calculating the mean of the time position of the left and right part of the chest – CH 3 and CH 4 – and assign this new calculated signal $t\_$-d$Z$/d$t$max34. This new calculated chest common channel could be used as a reference channel for calculating the PWV from the chest to a particular part of the body. The PWV to the left or right leg is thus assigned as PWV 34-7 and PWV 34-8, respectively.

Absolute SV values computed from bioimpedance signals are, unfortunately, dependent on subject-related physiological parameters such as weight and basal impedance.

$$SV = LVET \times VI \times VEPT,$$

where *VEPT* represents the volume of electrically participating tissue reflecting subject-related physiological parameters [2], *LVET* is the left ventricle ejection time, and *VI* is the peak velocity of blood flow

**Table 1:** Description of the tested group.

| | n | Age | Height (m) | Arm span (m) | Weight (kg) | BMI (kg/m²) |
|---|---|---|---|---|---|---|
| Group | 34 | 23.9±3.6 | 1.8±0.1 | 1.8±0.1 | 70.1±14.4 | 22.6±3.1 |
| | | 22.5 (21.0; 26.0) | 1.7 (1.7; 1.9) | 1.8 (1.7; 1.9) | 72 (59; 81) | 22.5 (20.4; 24.5) |
| Women | 18 | 24.7±4.6 | 1.7±0.1 | 1.7±0.1 | 59.9±9.8 | 21.6±3.2 |
| | | 22.5 (21.0; 28.0) | 1.7 (1.6; 1.7) | 1.7 (1.6; 1.7) | 59.5 (52; 69) | 21.3 (19.4; 23.7) |
| Men | 16 | 23.1±2.1 | 1.9±0.1 | 1.9±0.1 | 81.6±9.2 | 23.6±2.7 |
| | | 22.5 (21.0; 25.0) | 1.9 (1.8; 1.9) | 1.9 (1.8; 1.9) | 81.5 (74.5; 86.1) | 23.8 (21.3; 25.1) |

In the cells, the mean±STD and median (lower quartile; upper quartile) are mentioned.

in the aorta represented by the maximum amplitude of the negative first derivative of the impedance signal (-d*Z*/d*t*max).

*LVET* and *VI* are two parameters crucial for the comparison of relative changes of blood flow. *LVET* and *VI* are normally calculated by averaging the thoracic impedance signal from multiple heartbeats to eliminate noise, movement, respiratory effects, and other artefacts. The result is a value with reduced information about dynamic changes.

### Subject data

The tested group (group34) consisted of 34 healthy non-smoking volunteers – 18 young women and 16 young men aged 21–35 years. Table 1 shows the description of the tested group for statistical analysis. Information is also given about age, height, arm span, weight, and body mass index (BMI) for the whole group and then for the group of women and the group of men.

Four extra subjects were selected for diagnostic potential: a 53-year-old normotensive woman (W53-113/77), a 50-year-old hypertensive man (M50-152/77), a 57-year-old hypertensive woman (W57-170/83), and a 52-year-old normotensive woman who is a smoker (WS52-104/75). The fractional number in brackets is systolic BP/diastolic BP.

All subject measurements were approved by the St. Anne's University Hospital ethic committee no. 2G/2011, MZ-12, and fulfilled all the necessary regulations.

### Statistical analysis

The PWVs were calculated for each subject in the selected group at various places of measurement in the supine position and during a tilt test. Medians of PWVs for each subject were calculated from a 60-s period of supine and tilt excitation (last 60 s of the manoeuvre).

The null hypothesis (no difference of PWVs in the supine position and during the tilt test) was tested by a Wilcoxon paired test.

## Results

The MBM monitor is presented with examples of measurements during rest, tilting, exercise, and respiratory manoeuvres.

Here, we present results for the MBM with 18 channels. To demonstrate the results, we computed the absolute impedance value *Z* and its negative derivative -d*Z*/d*t*. Example data were collected from a normal healthy volunteer (male, 33 years old). The subject underwent an

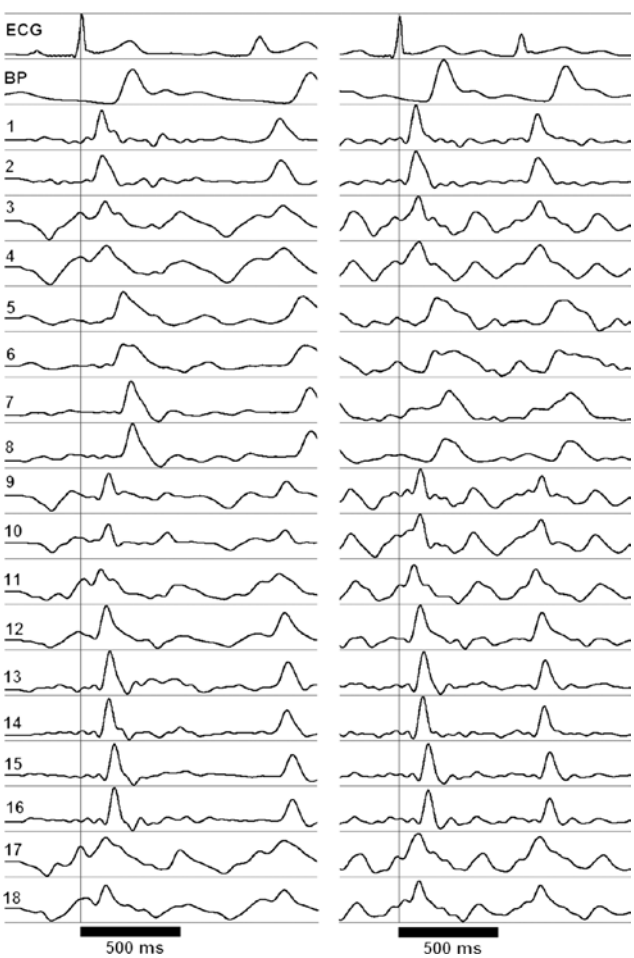


**Figure 5:** Average derivative magnitude of impedance signal, average from 100 beats, triggered to R wave maximum – vertical line.
ECG lead II, blood pressure BP, 1–18 negative derivative impedance signal, impedance signal in pass band 0.5–17 Hz. Left panel: rest, right panel: exercise.

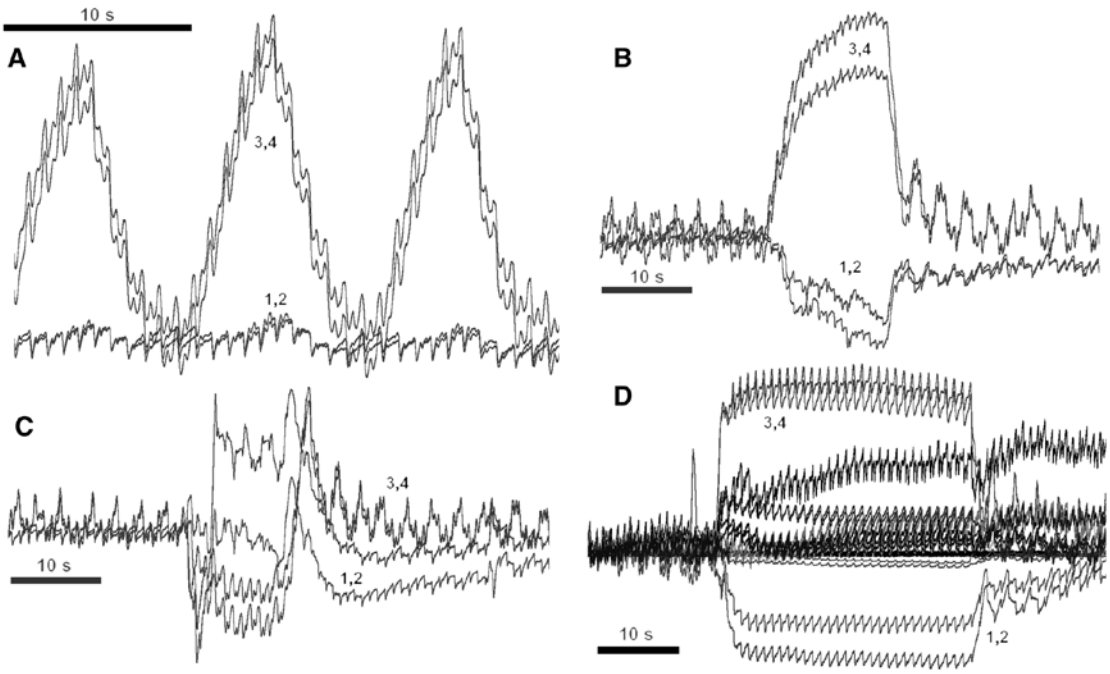


**Figure 6:** Respiration manoeuvres.
Raw magnitude of impedance signal from the thorax (3, 4) and carotids (1, 2).
(A) Paced breathing 6/min (10 s period); (B) Valsalva manoeuvre; (C) Mueller manoeuvre; (D) breath hold – complete set of MBM signals, thorax and carotids numbered.

exercise test (2 min rest, 5 min cycling in a horizontal position, 12 min rest), head-up tilt-table test (2 min rest in the supine position, 5 min 70° head-up tilt, 10 min rest in the supine position), 15 s Valsalva and Muller manoeuvres, and 30 s breath hold.

Averaging was used to obtain the best quality of the impedance signal shape. Figure 5 demonstrates the averaged ECG, BP, and -d$Z$/d$t$ from 18 locations during rest and exercise in steady states. Figures 6 and 7 show raw $Z$ signals that are influenced by overall blood volume in the investigated body part during tilting and breathing manoeuvres.

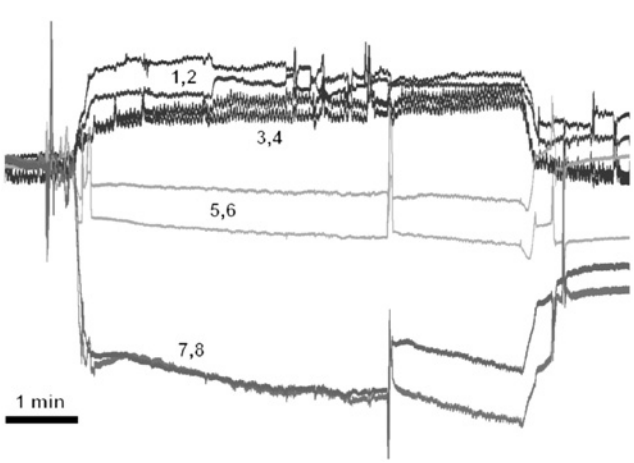


**Figure 7:** Head-up tilt-table test.
Raw magnitude of impedance signal from thorax (3, 4), carotids (1, 2) and legs (5, 6, 7, 8).

Averaged signals drawn in the same time window and expanded to the recovery phase started 1 min after the end of cycling are shown in Figure 8. This figure allows us to compare the shapes of the -d$Z$/d$t$ curves and their time distribution. Table 2 includes the detected time shift between the maximum of the $R$ wave and the maximum of the -d$Z$/d$t$ signals from Figure 8. There were also differences between the rest-cycling-rest phases and the time shift between the $R$ maximum and the systolic BP maximum and QT interval.

The results of measurement during the supine and tilt tests for all subjects of the tested group34 are presented in Table 3. Mean±standard deviation and median (lower and upper quartiles) are provided. Differences in PWV between manoeuvres (supine and tilt) to the lower limbs and changes of PWV in the lower and upper limbs are shown in Figure 9. Ranges, medians, and lower and upper quartiles of the differences of PWV between supine and tilt at various places of measurement are demonstrated in Figure 9. Statistically significant differences between

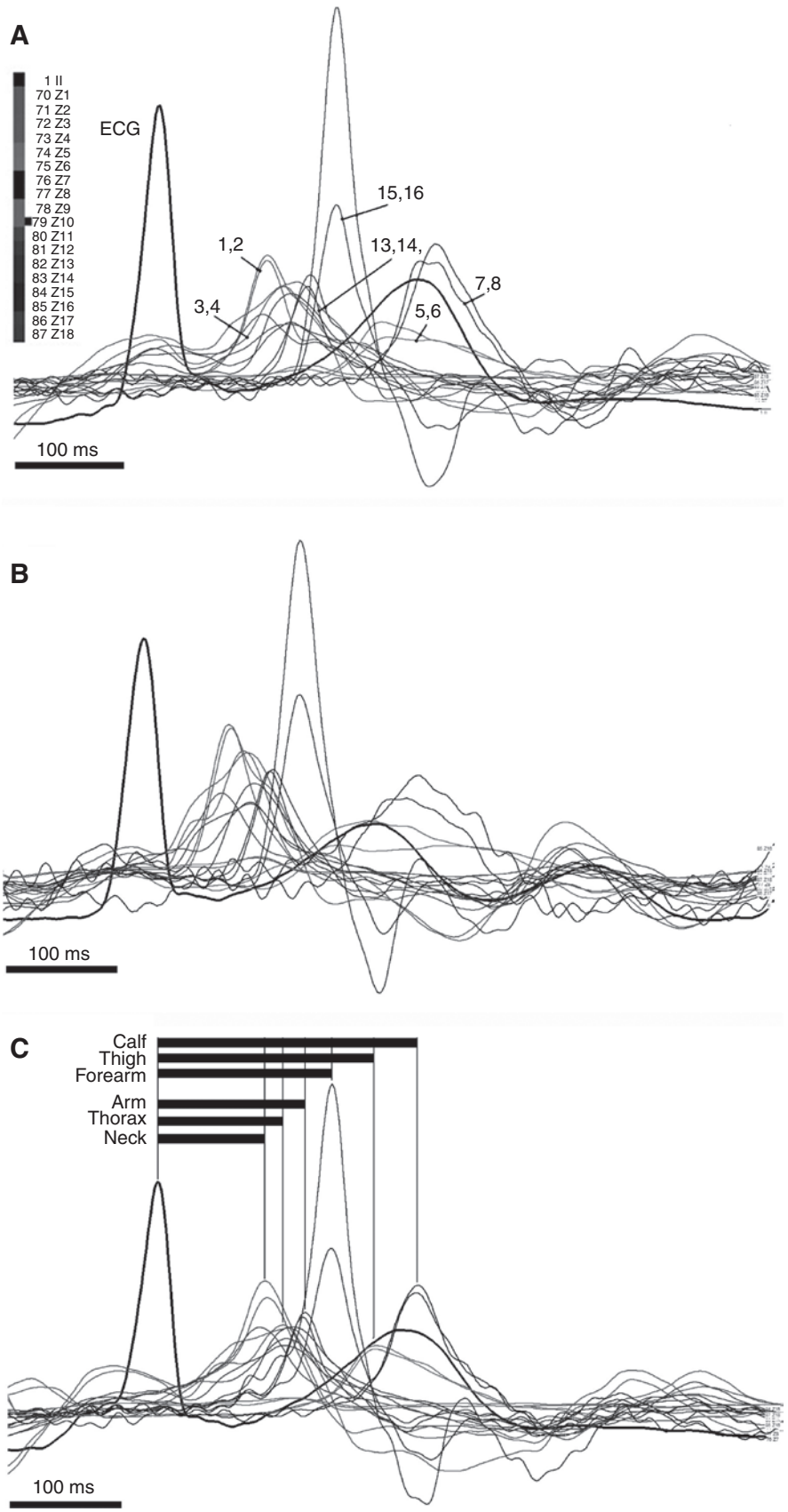


**Figure 8:** Averaged (from 100 beats) negative derivative magnitude of impedance signal from 18 locations. Pass band 0.5–45 Hz. (A) Rest, (B) exercise, and (C) rest started 1 min after the end of exercise.

**Table 2:** Detected time shift in milliseconds between the maximum of the R wave and the maximum of the -d*Z*/d*t* signal (Figure 8).

| Channel | 1 Rest | 2 Exercise | 3 Recovery | 1-2 | 3-2 | 1-3 |
|---|---|---|---|---|---|---|
| 1 | 98 | 78 | 98 | 20 | 20 | 0 |
| 2 | 98 | 76 | 96 | 22 | 20 | 2 |
| 3 | 114 | 88 | 112 | 26 | 24 | 2 |
| 4 | 126 | 92 | 118 | 34 | 26 | 8 |
| 5 | 202 | 184 | 194 | 18 | 10 | 8 |
| 6 | 208 | 176 | 194 | 32 | 18 | 14 |
| 7 | 244 | 246 | 232 | -2 | -14 | 12 |
| 8 | 254 | 232 | 232 | 22 | 0 | 22 |
| 9 | 132 | 102 | 122 | 30 | 20 | 10 |
| 10 | 132 | 102 | 122 | 30 | 20 | 10 |
| 11 | 94 | 70 | 90 | 24 | 20 | 4 |
| 12 | 120 | 98 | 118 | 22 | 20 | 2 |
| 13 | 138 | 114 | 130 | 24 | 16 | 8 |
| 14 | 138 | 112 | 130 | 26 | 18 | 8 |
| 15 | 162 | 140 | 154 | 22 | 14 | 8 |
| 16 | 162 | 140 | 154 | 22 | 14 | 8 |
| 17 | 116 | 96 | 112 | 20 | 16 | 4 |
| 18 | 120 | 96 | 114 | 24 | 18 | 6 |
| R-SBP | 250 | 218 | 240 | 32 | 22 | 10 |
| QT int | 364 | 332 | 352 | 32 | 20 | 12 |

Eighteen locations, R-SBP shift, QT interval. Before exercise (1, rest), during exercise (2, exercise), and during recovery phase (3, recovery). 1-2, 3-2, 1-3 – differences between time shifts.

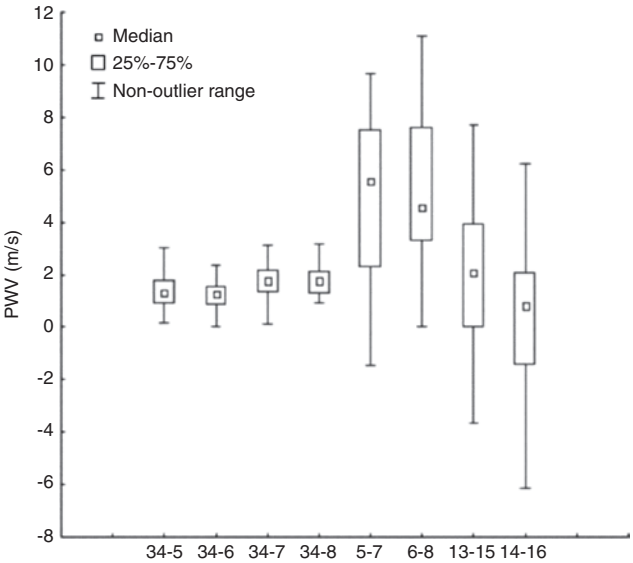


**Figure 9:** Differences in PWV between supine and tilt manoeuvres. 34-5 means difference in PWV between the chest and left thigh; 34-6 means difference in PWV between the chest and right thigh; 34-7 means difference in PWV between the chest and left calf; 34-8 means difference in PWV between the chest and right calf; 5-7 means difference in PWV between the left thigh and calf; 6-8 means difference in PWV between the right thigh and calf; 13-15 means difference in PWV between the left arm and forearm; and 14-16 means difference in PWV between the right arm and forearm.

supine and tilt were concluded in all cases ($p<0.001$) except PWV 14-16 in the upper right limb ($p=0.232$) – see Table 3.

An example of diagnostic potential is shown in Table 4. Here, the measured selected PWV for reference group34 of all subjects mentioned above is compared with four extra subjects – W53-113/77, M50-152/77, W57-170/83, and WS52-104/75. The two simple manoeuvres supine and tilt were selected.

**Table 3:** PWV during supine and tilt.

| | Supine | | Tilt |
|---|---|---|---|
| PWV 34-5 (m/s) | 5.6±0.7 | [a] | 7.0±1.1 |
| | 5.6 (5.1; 6.2) | | 6.9 (6.0; 7.9) |
| PWV 34-6 (m/s) | 5.6±0.8 | [a] | 6.9±1.1 |
| | 5.7 (5.1; 6.1) | | 6.7 (6; 7.8) |
| PWV 34-7 (m/s) | 6.7±0.7 | [a] | 8.6±1.0 |
| | 6.7 (6.2; 7.1) | | 8.3 (7.9; 8.9) |
| PWV 34-8 (m/s) | 6.7±0.7 | [a] | 8.5±1.1 |
| | 6.7 (6.2; 7.1) | | 8.3 (7.9; 8.8) |
| PWV 5-7 (m/s) | 11.8±2.9 | [a] | 16.7±3.4 |
| | 11.4 (10.0; 13.8) | | 17.5 (14.5; 19.4) |
| PWV 6-8 (m/s) | 11.4±2.0 | [a] | 16.7±3.4 |
| | 11.4 (10.0; 13.1) | | 16.9 (15.0; 18.3) |
| PWV 13-15 (m/s) | 11.0±3.2 | [a] | 13.7±4.5 |
| | 10.0 (8.8; 13.6) | | 12.8 (10.0; 16.9) |
| PWV 14-16 (m/s) | 9.9±2.6 | NS | 10.6±3.0 |
| | 9.2 (8.7; 10.9) | | 10.4 (8.8; 12.2) |

In the cells, the mean±STD and median (lower quartile; upper quartile) are mentioned. [a]$p<0.001$; NS, non-significant.

# Discussion

## MBM benefits

Several variations of electrode configurations and CO equations have been presented over the years to improve the ICG method. Although much work has already been done, the development of ICG is still based principally on the same concept introduced decades ago. ICG is currently used to measure haemodynamic parameters by means of commercial devices. However, the accuracy and reproducibility of calibrated CO is the subject of much discussion and probably has no solution. Full-body MBM, in contrast to thoracic measurement, offers an extensive set of signals. It enables more precise estimation not only of *LVET* and -d*Z*/d*t*max values beat-to-beat, but also pulse pressure propagation and signal morphology change in locations, and thus it provides a new possibility for

**Table 4:** PWV to and in the lower extremities during supine and tilt in m/s, and PWV during tilt normalised to supine position in % (tilt norm).

| | Group34 | W53-113/77 | M50-152/79 | W57-170/83 | WS52-104/75 |
|---|---|---|---|---|---|
| Supine | | | | | |
| PWV 34-5 | 5.6±0.7 | 7.4 | 8.4 | 12.8 | 7.0 |
| PWV 34-6 | 5.6±0.8 | 7.8 | 8.4 | 13.0 | 6.9 |
| PWV 34-7 | 6.7±0.7 | 8.6 | 10.0 | 12.0 | 9.1 |
| PWV 34-8 | 6.7±0.7 | 8.6 | 9.7 | 11.8 | 8.8 |
| PWV 5-7 | 11.8±2.9 | 12.9 | 14.6 | 16.0 | 20.1 |
| PWV 6-8 | 11.4±2.0 | 10.6 | 13.7 | 18.5 | 18.0 |
| Tilt | | | | | |
| PWV 34-5 | 7.0±1.1 | 12.9 | 9.6 | 21.1 | 13.3 |
| PWV 34-6 | 6.9±1.1 | 12.8 | 8.9 | 22.4 | 13.1 |
| PWV 34-7 | 8.6±1.0 | 14.4 | 10.9 | 15.6 | 15.3 |
| PWV 34-8 | 8.5±1.1 | 14.3 | 10.9 | 16.8 | 15.1 |
| PWV 5-7 | 16.7±3.4 | 20.0 | 15.8 | 19.2 | 21.1 |
| PWV 6-8 | 16.7±3.4 | 18.0 | 18.6 | 22.3 | 21.1 |
| Tilt norm (%) | | | | | |
| PWV 34-5 | 125.1 | 174.3 | 114.3 | 164.8 | 190.0 |
| PWV 34-6 | 122.8 | 164.1 | 106.0 | 172.3 | 189.9 |
| PWV 34-7 | 127.7 | 167.4 | 109.0 | 130.0 | 168.1 |
| PWV 34-8 | 126.7 | 166.3 | 112.4 | 142.4 | 171.6 |
| PWV 5-7 | 141.5 | 155.0 | 108.2 | 120.0 | 105.0 |
| PWV 6-8 | 146.5 | 169.8 | 135.8 | 120.5 | 117.2 |

Comparison between the reference group of healthy volunteers (group 34) and a normotensive 53-year-old woman (W53-113/77), a hypertensive 50-year-old man (M50-152/77), a hypertensive 57-year-old woman (W57-170/83), and a normotensive 52-year-old woman who is a smoker (WS52-104/75).

analysing blood flow in the extremities, neck, and thorax. Moreover, parameters related to time shifts do not require additional hard-defined coefficients, except for the limb length of the subject.

However, a great deal of measurement should be performed for the absolute blood flow in l/min in the extremities, neck, and part of the chest and compared with another blood flow method such as Doppler sonography. The bioimpedance of each channel has to be normalised to the distance of the scanning electrodes and the cross-section of the vein in the investigated area. The use of an empirical constant will also probably be necessary, as in the evaluation of CO.

Nevertheless, many measurements based on relative blood flow volume and/or excited blood flow changes and/or morphology of the bioimpedance curve or its derivatives can be performed directly, for example, measurements on a tilt table, on a treadmill, or on a stationary bicycle, where changes in blood flow are important. Comparing blood flow in the geminate organs and extremities of one body can also help during the diagnosis of particular diseases. Pulse wave analysis is also possible, and can be evaluated for each scanning channel except channels associated with the heart. This presumes the exact recording of electrode topology, which must be performed during each examination. Vein stiffness can be estimated from pulse wave analysis. The data from all channels, together with detailed vein stiffness information, can help in improving the accuracy of the calculation of CO and other parameters based on bioimpedance chest measurements.

The MBM frequency bandwidth is higher in comparison with non-invasive photoplethysmography BP measurement (Finapres, Portapres, Finometer, Ohmeda Medical, Englewood, CO, USA). The MBM shape is more detailed and allows a more precise analysis of impedance signal shape. A large amount of information about the state of the arteries in the extremities can be expected to be found.

## Three current sources

The three independent current sources with different but very close frequencies (49, 50, and 51 kHz) enable us to map blood flow in the full human body simultaneously at approximately the same conditions. The first and the second current sources are dedicated to the left and right body part from the neck (carotids) to the ankle in vertical direction. The third current source is dedicated to the upper extremities and the upper part of chest in horizontal direction. With less than three current sources, full-body blood flow mapping including all extremities, chest, and neck cannot be achieved. With two current sources, it is possible to measure either from the neck to the calf and not the hands or from the wrists to the calf and not the neck; the full body cannot be mapped. The information in the particular impedance channel is affected by the localisation of the voltage electrodes and by the frequency setting of the channel only. In the proposed MBM, the channels are thus independent with no redundancy. The only place where a crosstalk of impedance channel information could occur is the chest and the abdomen. This is caused by the particular electric current flow pathway through the chest and the abdomen and their electrical conductivity, which cannot be affected from the outside. There, the left and right current pathways are very similar. The influence of the right current source is not detected by the left channels in any case. However, in the left chest and abdomen channels, information could also be from the right part of the chest and abdomen because the current from the left current source could flow there. The same is valid for the right chest and abdomen channels.

## Example of an application

The MBM allows, for example, detection of limb perfusion and arterial elasticity change depending on blood filling. The simultaneous measurement of invasive arterial BP and MBM in the same part of the body (the forearm, for example) allows the analysis of differences between impedance signal shape and pressure curve shape, and analysis of the expansion of arteries for various arterial pressures. It will, therefore, be able to derive a correction function for the accurate calculation of blood flow and CO from the impedance signal.

Measurements with excitations (tilt table, exercise, respiration manoeuvres) make it possible to analyse and compare dynamic haemodynamic changes during rest-excitation-recovery stages. Figure 6 shows a comparison of the impedance signal from the thorax and carotids. Figure 6A demonstrates differences during deep slow breathing. The signal from the thorax is strongly contaminated by respiration-induced impedance change, while the carotids, in contrast, reflect only arterial pressure change. Figure 6 (B and C) demonstrates 15-s Valsalva (VM) and Muller (MM) manoeuvres. VM (exhalation against closed airway, positive pressure in lungs) causes impedance increase in the thorax (a reduction of blood volume and also artificial impedance increase) and impedance decrease in the neck (an increase in blood volume). The MM (the reverse of VM, negative pressure in the lungs) causes a decrease of impedance in the thorax (an increase in blood volume and also an artificial impedance decrease) and an increase of impedance in the neck (a decrease in blood volume, here non-symmetric). Figure 6D demonstrates breath hold at all 18 locations. The impedance from the thorax and the neck is similar to VM.

Table 2 includes examples of changes to pulse wave propagation between the rest state before exercise, during exercise, and in the rest state 1 min after exercise. There is an interesting difference (1–3 rest before exercise – recovery) in the legs, particularly in the calves. There is a minimal difference in the neck, thorax, and body. The result is the finding that the PWV is higher in the legs during rest after exercise than during resting. This reflects the increased blood circulation in the legs after exercise. Continual vessel recovery can be analysed if we reduce the window size for averaging.

It is possible to analyse the accumulation of blood in the extremities when measuring during head-up tilt-table tests or any vertical change of body position. Figure 7 demonstrates the different blood distribution during head-up tilt. The most significant decrease in impedance (blood volume increase) is seen in the calves – higher than that in the thigh. There is an impedance increase (blood volume decrease) in the thorax and the neck. There is evident blood accumulation in the legs, particularly in the calves, and reduction of blood volume in the thorax and neck.

The statistical analysis shows us that a bioimpedance-based method for PWV could effectively map the properties of blood flow. It is evident from Figure 9 that changes of PWV from the chest to parts of the lower limbs between the supine and tilt positions are significant in both legs. The tilt position causes blood filling in the legs and then an increase of PWV. Also, the PWV in the upper and lower limbs is significant; the PWV is not significant only in the right limb. This is due to its different position – this limb was placed perpendicular to the body for the purpose of BP measurement, while the left limb was lying collateral, which leads to less blood filling during the tilt manoeuvre. The PWV is higher during the tilt manoeuvre because the limbs are filled with more blood than in the supine position and the artery wall is exposed to more pressure and is stiffer.

We can see from Table 4 that the PWVs either in the lower extremities or to the lower extremities is significantly higher for the investigated subjects with hypertension: a 50-year-old man with BP 152/79 (M50-152/79) and a 57-year-old woman with BP 170/83 (W57-170/83) in rest in the supine position in comparison to the reference group (group34). The PWVs are affected by age and hypertension (which has a greater influence). The 53-year-old woman with a normal BP (W53-113/77) has only slightly higher PWVs than the reference group of volunteers, which is due to age. We found a similar result in the case of a 52-year-old female smoker with a normal BP (WS52-104/75), but only in the case of PWVs to the calves and thighs. The PWV in the legs (left and right) is, however, much higher than in the case of the reference group. This fact is extremely important and indicates changes of artery compliance in the lower extremities. During tilting, all the PWVs increased in the case of group34. Similar behaviour can be found in the case of W53-113/77. The only difference is that the absolute value of PWV is higher due to age. Subjects M50-182/79 and W57-170/83 with hypertension have similar changes in PWVs, but the absolute value of PWV is higher than in the case of group34. Hypertension is the main reason for phenomena such as in the supine position. The female smoker WS52-104/75 has changes in PVW to the leg similar to the previously mentioned subjects. The big difference in the behaviour of the PWVs is in the leg (PWV 5-7 and PWV 6-8). The PWVs were not changed and remained very high. The arteries in the legs lost

compliance considerably, and the PWV was the same during supine and tilt. The compliance of the artery in the chest remains the same in this case. This is probably caused by cigarette smoking. Standard measurement of the PWV between the chest and lower extremities is not able to recognise this problem. This fact increases the necessity for PWV measurement at certain parts of the body to reveal the problematic part that may be hidden.

## Conclusion

We have demonstrated multichannel bioimpedance signal measurement. We have also described the method for its measurement and patient connection. The MBM device can provide a high-quality, complex-valued continuous bioimpedance signal on multiple channels simultaneously. These signals can be further used in many fields of diagnosis of cardiovascular and blood system diseases. We have shown a full-body (18 channels) impedance measurement and its derivatives, together with various processing during patient tilting and during exercise.

The proposed MBM could help in improving the accuracy of CO measurement and, thanks to its full-body simultaneous blood flow monitoring and the high quality of its output signals, could provide new data for haemodynamic and blood flow analysis, particularly in the measurement of PWV in a particular part of the body.

**Acknowledgments:** This work was supported by research projects from the Ministry of Education, Youth and Sports of the Czech Republic (MEYS CR) (LO1212); its infrastructure by MEYS CR and European Commission (EC) (CZ.1.05/2.1.00/01.0017); the European Regional Development Fund – Project FNUSA-ICRC (No. CZ.1.05/1.1.00/02.0123); P102/12/2034 from the Grant Agency of the Czech Republic; and RVO: 68081731 from the Academy of Sciences of the Czech Republic.

## References

[1] Bernstein DP. Impedance cardiography: pulsatile blood flow and the biophysical and electrodynamic basis for the stroke volume equations. J Electr Bioimp 2010; 1: 2–17.
[2] Bernstein DP, Lemmens HJM. Stroke volume equation for impedance cardiography. Med Biol Eng Comput 2005; 43: 443–450.
[3] Bourne JR (ed.). Bioelectrical impedance techniques in medicine. Crit Rev Biomed Eng 1996; 24: 223–678.
[4] Cachovan M, Linhart J, Prerovsky I. Morphology of pulse wave curve from various segments of lower limb in man. Angiology 1968; 19: 381–392.
[5] Carter B, Mancini R (eds.). OP AMPS for everyone. 3rd ed. Oxford: Elsevier Inc. 2009.
[6] Cotter G, Schachner A, Sasson L, Dekel H, Moschkovitz Y. Impedance cardiography revisited. Physiol Meas 2006; 27: 817–827.
[7] Engoren M, Barbee D. Comparison of cardiac output determined by bioimpedance, thermodilution, and the Fick method. Am J Crit Care 2005; 14: 40–45.
[8] Fortin J, Bojic A, Habenbacher W, Heller A, Hacker A. Non-invasive beat-to-beat cardiac output monitoring by an improved method of transthoracic bioimpedance measurement. Comput Biol Med 2006; 36: 1185–1203.
[9] Henry IC, Bernstein DP, Banet MJ. Stroke volume obtained from the brachial artery using transbrachial electrical bioimpedance velocimetry. In: 34th Annual International Conference of the IEEE EMBS (San Diego) 2012: 142–145.
[10] Honzikova N, Labrova R, Maderova E, et al. Influence of age, body mass index, and blood pressure on the carotid intima-media thickness in normotensive and hypertensive patients. Biomed Tech (Berl). 2006; 51: 159–162.
[11] Keren H, Burkhoff D, Squara P. Evaluation of a noninvasive continuous cardiac output monitoring system based on thoracic bioreactance. Am J Physiol Heart Circ Physiol 2007; 293: 583–589.
[12] Kerlan JE, Sawhney NS, Waggoner AD, et al. Prospective comparison of echocardiographic atrioventricular delay optimization methods for cardiac resynchronization therapy. Heart Rhythm 2006; 3: 148–154.
[13] Koivistoinen T, Kööbi T, Jula A, et al. Pulse wave velocity reference values in healthy adults aged 26–75 years. Clin Physiol Funct Imaging 2007; 27: 191–196.
[14] Kööbi T, Kaukinen S, Ahola T, Turjanmaa VMH. Non-invasive measurement of cardiac output: whole-body impedance cardiography in simultaneous comparison with thermodilution and direct oxygen Fick methods. Intensive Care Med 1997; 23: 1132–1137.
[15] Kubicek WG, Karnegis JN, Patterson RP, Witsoe DA, Mattson RH. Development and evaluation of an impedance cardiac output system. Aerosp Med 1966; 37: 1208–1212.
[16] Leonhardt S, Cordes A, Plewa H, et al. Electric impedance tomography for monitoring volume and size of the urinary bladder. Biomed Tech (Berl). 2011; 56: 301–307.
[17] Patterson RP. Impedance cardiography: what is the source of the signal? J Physics 2010; 220: 012118.
[18] Rui-zhe J, Xiao-mei L, Xin W, Hai-qing W. Relationship between cardiovascular function and fetal growth restriction in women with pre-eclampsia. Int J Gynecol Obstet 2010; 110: 61–63.
[19] Schmidt C, Theilmeier G, Van Aken H, et al. Comparison of electrical velocimetry and transoesophageal Doppler echocardiography for measuring stroke volume and cardiac output. Br J Anaest 2005; 95: 603–610.
[20] Schwingenschuh S, Hajnsek M, Scharfetter H, et al. Skin impedance measurements support *ex-vivo* penetration studies for topical applied drugs. Biomed Tech (Berl). 2013; 58 (Suppl. 1). DOI: 10.1515/bmt-2013-4420.
[21] Stanley AWH, Herald JW, Athanasueeas CL, Jacob AC, Bartolucci AA, Tsoglin A. Multi-channel electrical bioimpedance: a non-invasive method to simultaneously measure cardiac

output and individual arterial limb flow in patients with cardiovascular disease. J Clin Monit Comput 2009; 23: 243–251.
[22] Viscor I, Vondra V, Halamek J. Two-channel high dynamic range bioimpedance monitor for cardiography. IFMBE Proc 2007; 17: 225–228.
[23] Woltjer HH, Bogaard HJ, Scheffer GJ, van der Spoel HI, Huybregts MA, de Vries PM. Standardization of noninvasive impedance cardiography for assessment of stroke volume: comparison with thermodilution. Br J Anaest 1996; 77: 748–752.
[24] Zhao Z, Vogt B, Falkenberg C, Weiler N, Möller K, Frerichs I. Customized electrical impedance tomography based analysis of regional lung function: a feasibility study. Biomed Tech (Berl) 2013; 58 (Suppl. 1). DOI 10.1515/bmt-2013-4131.